Tissue-mimicking agar/gelatin materials for use in heterogeneous elastography phantoms

Ernest L Madsen, Maritza A Hobson, Hairong Shi, Tomy Varghese and Gary R Frank

Department of Medical Physics, University of Wisconsin, 1300 University Avenue, Room 1530, Madison, WI 53706, USA

E-mail: elmadsen@wisc.edu

Abstract

Five 9 cm × 9 cm × 9 cm phantoms, each with a 2-cm-diameter cylindrical inclusion, were produced with various dry-weight concentrations of agar and gelatin. Elastic contrasts ranged from 1.5 to 4.6, and values of the storage modulus (real part of the complex Young's modulus) were all in the soft tissue range. Additives assured immunity from bacterial invasion and can produce tissue-mimicking ultrasound and NMR properties. Monitoring of strain ratios over a 7 to 10 month period indicated that the mechanical properties of the phantoms were stable, allowing about 1 month for the phantom to reach chemical equilibrium. The only dependable method for determining the storage moduli of the inclusions is to make measurements on samples excised from the phantoms. If it is desired to produce and accurately characterize a phantom with small inclusions with other shapes, such as an array of small spheres, an auxiliary phantom with the geometry of the cylindrical inclusion phantoms or the equivalent should be made at the same time using the same materials. The elastic contrast can then be determined using samples excised from the auxiliary phantom. A small increase of about 10% in volume of the cylindrical inclusions occurred—a tolerable increase. Interestingly, the smallest increase (about 5%) occurred in the phantom with the largest elastic contrast.

1. Introduction

Phantoms for use in elastography have been produced in many laboratories over the last decade. Usually the phantoms produced are *ad hoc*, and there is little concern for long-term stability of physical properties or for immunity from deterioration due to environmental variations (e.g. temperature). Also, although values of elasticity properties of materials are reported, little attention has been given to the degree to which elastography phantom materials also

possess tissue-mimicking (TM) values of ultrasound and/or NMR properties. For example, if the ultrasound attenuation coefficient is a reasonable approximation for a target tissue, but the propagation speed is 900 m s^{-1} instead of the 1540 m s^{-1} assumed by the scanner, then elastographic performance might appear to be acceptable to 15 cm depth at a nominal 7 MHz scanner frequency instead of to a depth of 15 cm $\times$ 900/1540 $\approx$ 9 cm. A thorough review of the literature on elastography phantoms has been included in a recent publication (Madsen *et al* 2003); thus, a review of only published work most closely related to that reported in this paper is given here.

Mixtures of agar and gelatin were used in phantoms for use in elastography by de Korte *et al* (1997). Three homogeneous samples were made with 1%, 2% and 3% dry-weight agar, the dry-weight concentration of gelatin being 8% in all three. The samples were congealed by immersing in ice water, and no cross-linking agent was employed to elevate the melting point of the final materials above that of gelatin; the melting point of typical gelatins is about 32 °C. The 'compressibility modulus' was monitored for a 4 h period following congealing; there was no long-term stability study done.

Other investigators have produced heterogeneous phantoms using agar/gelatin mixtures (Kallel *et al* 2001). The dry-weight gelatin concentration was different in the background materials than in the inclusions, and as a result of osmosis the diameters of the inclusions changed considerably over a period of 2 weeks. Similar phantoms, in which variations in the dry-weight concentration of gelatin were employed to cause elastic contrast, were produced by Gao *et al* (1995). As in the case of the phantoms made by Kallel *et al* (2001), osmosis due to differences in dry-weight gelatin concentrations would preclude long-term stability.

It has been observed in our laboratory that an aqueous agar background does not change size or shape significantly even though the dry-weight agar concentration of the inclusion material differs from that of its surroundings. This geometric stability does not exist for gelatin inclusions in gelatin surroundings, i.e., if the initial dry-weight gelatin concentration in the inclusion is greater than or less than that in the surroundings, the inclusion will increase or decrease in volume, respectively, presumably due to osmosis. Thus, for an aqueous mixture of agar and gelatin, a reasonable expectation is that the shape and size of inclusions will not change if the dry-weight gelatin concentration is the same in the inclusions as in the surroundings, while the dry-weight agar concentration in inclusions can be different than in the surroundings. When the dry-weight gelatin concentration is different in the inclusions than in the surroundings—as in the case of Kallel *et al* (2001)—it is reasonable that the size of an inclusion would change with time due to osmosis.

Before the advent of elastography, Madsen *et al* (1991) reported a low MR contrast spherical lesion phantom for use in MRI where the dry-weight gelatin concentration was uniform throughout, but the dry-weight agar concentration was 2.7% in the background and lower in the spheres. The lower agar concentration produced higher values of the longitudinal relaxation time (T_1) and the transverse relaxation time (T_2) in the spheres than in the background resulting in clinically relevant MR (object) contrast. (Object contrast depends on bulk material parameters; thus, in this case the ratio of T_2 for the sphere material divided by the T_2 for the background material might be considered the T_2 object contrast.) The dry-weight agar concentration in one set of spheres was 1.35% and in another set of spheres was 2.02%; thus, the object contrast in the former case (1.35% agar) was greater than in the latter case (2.02% agar). Each set contained spheres ranging in diameter from 2 mm through 9.5 mm; thus, the test for the MRI unit was to determine the smallest sphere diameter of each contrast; the phantom might be referred to as a spherical lesion 'contrast-detail' phantom. The phantom also contained formaldehyde throughout to cross-link the gelatin, raising the melting point to 78 °C where the agar component melts.

Long-term stability of lesion diameters and T_2 relaxation times in the 'contrast-detail' phantom was assessed with two auxiliary phantoms made specifically for testing long-term stability of those parameters. One phantom contained two 3.18-cm-diameter spheres, one of each object contrast found in the 'contrast-detail' phantom. The second phantom was identical except that the two spheres were 0.95 cm in diameter. The larger diameters allowed T_2s in the spheres and in the background to be measured directly in the phantom with a GE Signa clinical MR unit. Three glass bottles, each containing one of the three types of material, were produced at the time the auxiliary phantoms were made, using the same materials. T_2s were measured in these three uniform materials at the same time T_2s were measured in the two auxiliary phantoms. Thus, any drift in T_2 values due to the direct contact of different materials in the auxiliary phantoms could be monitored. The diameters of the spheres were also monitored by making MR images with the scan planes through the centres of the spheres. T_2s in the auxiliary phantoms and in the corresponding uniform materials in the glass bottles remained within a few per cent of one another over the times monitored (14 weeks in the case of the 3.18-cm sphere phantom and 20 months in the case of the 0.95-cm sphere phantom). Also, over the periods monitored the diameters of the spheres on MR images did not change perceptibly, indicating long-term stability of geometry.

As in the Madsen *et al* case, Plewes *et al* (2000) produced an agar/gelatin phantom in which the agar concentration was different in the inclusion than in the background, while the gelatin concentration was the same throughout the phantom. Thus, the size and shape of the inclusion would likely have been temporally stable. However, neither elastic nor NMR properties were monitored over time to assess long-term stability, and apparently there was no cross-linking agent used to raise the melting point above that of the gelatin *per se*. (Without cross-linking our gelatin melts at 32 °C.)

Since higher agar concentrations produce noticeably stiffer materials, it is reasonable to expect that higher agar concentrations in agar/gelatin materials will correspond to higher Young's moduli. In this paper, we report on the long-term stability of inclusion geometries and on the stability of Young's moduli and elastic contrasts for heterogeneous phantoms in which the gelatin concentration is constant throughout the agar/gelatin mixtures in each phantom, while the agar concentration differs between inclusion and background. The phantoms consist of 9 cm × 9 cm × 9 cm cubes of background material with 2-cm-diameter cylindrical inclusions. The materials have NMR relaxation times, T_1 and T_2, which mimic soft tissues. Without appropriate additives, the ultrasound propagation speeds and attenuation coefficients are lower than those typical for soft tissues, and NMR T_1s are higher than those in most soft tissues. Values of propagation speeds can easily be elevated with addition of solutes and tissue-mimicking values of attenuation coefficients can be produced with addition of microscopic particulates. The latter solutes and particulates can be chosen to affect the NMR relaxation times negligibly. Independently, NMR T_1s can be lowered with addition of a Cu^{2+} salt plus EDTA (ethylene diamine tetraacetic acid), the latter to assure long-term stability (Rice *et al* 1998).

Extensive testing of the long-term stability of inclusion geometries and elastic properties of component materials is reported for a set of five heterogeneous agar/gelatin phantoms.

2. Materials and production methods

Each agar/gelatin component in the phantom contains (dissolved) granulated agar (Fisher Scientific, Pittsburgh, PA, cat. no. BP1423), '200 bloom' gelatin derived from calf skin (Vyse Gelatin Company, Schiller Park, IL), 18 MΩ cm deionized water, $CuCl_2$-$2H_2O$, EDTA-tetra Na hydrate [ethylenediaminetetraacetic acid tetrasodium hydrate] (Aldrich,

Milwaukee, WI, cat. no. E2,629–0), NaCl, an antibacterial agent (as described in detail later) and HCHO (formaldehyde). The gelatin likely is responsible for the bonding that forms between inclusions and background materials. Increased dry-weight concentration of agar produces greater stiffness (higher Young's modulus). EDTA forms a chelate with the Cu^{2+} ions, sufficient EDTA being present that all Cu^{2+} ions are attached to EDTA. The purpose of forming the chelate is to allow the Cu^{2+} to remain mobile, thus allowing controlled lowering of the T_1 relaxation time. (Without EDTA, the Cu^{2+} ions slowly become immobilized by attaching to the gelatin molecules, thus eliminating their T_1-lowering capacity.) NaCl is present in sufficient concentration to produce tissue-like NMR coil loading. Formaldehyde cross-links gelatin molecules raising the melting point of the material to over 65 °C. In one phantom, prevention of fungal and bacterial invasion was accomplished with 1.0 g l^{-1} of thimerosal, a mercury-containing compound used in earlier elastography phantoms (Madsen *et al* 2003); in the other phantoms prevention was done with a less toxic preservative called Germall-plus® (International Specialty products, Wayne, NJ, USA) which contains no mercury and is therefore environmentally more acceptable. Also, some phantoms contain rather high concentrations of microscopic glass beads to increase ultrasonic attenuation and backscatter to tissue-like levels.

For the five heterogeneous phantoms reported in this paper (referred to as phantoms A, B, C, D and E), the concentrations of the various components differ from one phantom to another; however, within any one phantom the dry-weight gelatin concentration is constant throughout, stiffness differences resulting primarily from differences in dry-weight agar concentrations.

The procedure for making the agar/gelatin materials is presented in the form of an example; namely, the production of 1.2 l of the background material in phantom B. Other agar/gelatin materials are made in the same way with differences in concentrations of one or more components. First, quantities of molten gelatin and molten agar are made. Using different beakers, 50.4 g of dry gelatin and 64.5 g of glass beads (Potters Industries, Parsippany, NJ, USA; catalog number 4000E) are added to 460 cc of 18 MΩ cm room-temperature distilled water, and 16.33 g of dry agar are added to 800 cc of 18 MΩ cm room-temperature distilled water. The two mixtures are heated in double boilers; thus, the beakers are not in direct contact with the heat sources to avoid overheating at the bottoms of the beakers. After the two materials have clarified (Usually clarification has occurred when the temperature has risen to the 90 °C range.), 460 cc of the molten gelatin and 720 cc of the molten agar are mixed together in another beaker. (The volume per cents are approximately 40% and 60%, respectively, for all agar/gelatin materials reported here.) While the mixture is at 70–80 °C, 4.1 g of EDTA-tetra Na hydrate is completely dissolved into it. Then 1.4 g of $CuCl_2$-$2H_2O$ and 9.6 g of NaCl are dissolved. By partially immersing the beaker in cold water and stirring, the mixture is cooled to 50 °C, and 18 g of Germall-plus are dissolved into it. The mixture is then cooled to 36 °C and 3.0 cc of formalin solution is mixed in. (Note that formalin solution is 37% formaldehyde.) At this point, the molten agar/gelatin is ready to be poured into a mould for cooling and congealing overnight to room temperature.

The glass beads present in the materials contribute to both scattering and attenuation. The 4000E beads have the following typical diameter distribution: 10% are less than 5 μm, 50% are less than 18 μm and 90% are less than 45 μm. The mean diameter of these beads is typically 20 μm.

2.1. Heterogeneous phantoms

Each phantom produced consists of a 9 cm × 9 cm × 9 cm cube of background material with a 2-cm-diameter cylindrical inclusion which is perpendicular to two sides. A diagram
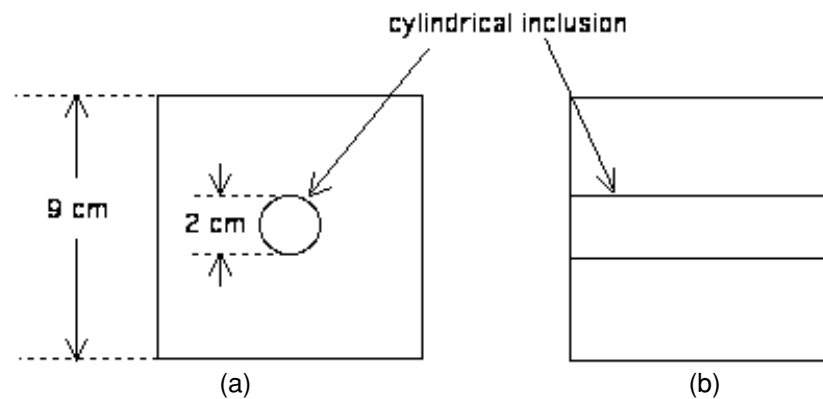
Figure 1. Heterogeneous phantom geometry used in long-term stability tests: (a) view with the axis of the cylindrical inclusion perpendicular to the figure; (b) view with the axis parallel to the plane of the figure.

Table 1. Dry-weight per cents of the various components in the phantoms. The weight per cent of 18 MΩ cm water is not shown since it just makes up the remainder. The gelatin concentrations in the background and inclusion of any one phantom are the same in the agar/gelatin when glass beads are excluded; because of the significant difference in glass bead concentrations between background and inclusions in phantoms D and E, the *weight-per cent* of gelatin, e.g., gelatin is higher in the inclusion than in the background.

Material	Agar	Gelatin	$CuCl_2$-$2H_2O$	EDTA tetra-Na hydrate	NaCl	HCHO	Germall plus	Glass bead scatterers
Phantom A background	1.17	3.60	0.113	0.33	0.77	0.24	–	4.6
Phantom A inclusion	3.53	3.60	0.113	0.33	0.77	0.24	1.45	5.6
Phantom B background	1.17	3.60	0.113	0.33	0.77	0.24	1.45	4.6
Phantom B inclusion	3.53	3.60	0.113	0.33	0.77	0.24	1.45	5.6
Phantom C background	1.17	5.52	0.113	0.33	0.77	0.24	1.45	4.4
Phantom C inclusion	3.53	5.52	0.113	0.33	0.77	0.24	1.45	5.4
Phantom D background	1.17	5.52	0.113	0.33	0.77	0.24	1.45	4.4
Phantom D inclusion	3.64	5.70	0.116	0.34	0.80	0.25	1.50	0.0
Phantom E background	1.11	4.80	0.114	0.33	0.77	0.32	1.45	3.4
Phantom E inclusion	3.44	4.92	0.116	0.34	0.79	0.33	1.49	0.75

is shown in figure 1. The cylinder is centred in the phantom, i.e., the axis of the cylinder is 4.5 cm from four surfaces of the cubic phantom. The dry-weight gelatin concentration is constant throughout each phantom, including background and inclusion. The concentration for each component in the phantoms is shown in table 1.

Each phantom is produced in two basic steps. First, the background is made. The mould to receive the molten background material is an acrylic box open at opposite ends over which Saran Wrap is epoxied. The barrel of a sawed-off 30 cc hypodermic syringe is epoxied into a hole in one acrylic wall near one corner of the box. An acrylic cylindrical rod passes through holes in opposite sides of the box. 'Five-minute' epoxy (3M Scotch Weld DP100, 3M Industrial Adhesives and Tapes, St. Paul, MN, USA) ensures a seal between the rod and the holes in the box. This epoxy forms an adequate bond with acrylic but can be removed rather easily with a knife. Prior to gluing on the last Saran Wrap layer, all surfaces which will be in contact with the molten background material are coated with a thin layer of petrolatum.

This layer allows clean removal of the stainless steel rods and then removal of the completed background from the mould.

After the 40 °C molten background material has been introduced into the mould and syringe barrel through the projecting syringe barrel, the syringe piston is inserted into the syringe barrel and rubber bands attached to maintain positive gauge pressure on the material as it congeals. Note that before the molten background material is poured in, acrylic constraining plates are taped over the Saran Wrap sides to assure flatness of those sides of the background material. The entire apparatus is mounted on a rotator so that rotation at 2 rpm about a horizontal axis occurs throughout the congealing period; thus, gravitational sedimentation of glass beads, etc, is avoided.

After about 24 h, formaldehyde cross-linking will have raised the melting point of the material above 60 °C. Then the second production step is carried out, namely, production of the inclusion. The epoxy seals around the acrylic rod are removed and the rod is withdrawn. The hole in the gel is then quickly and gently cleaned with Kimwipes® (Kimberly-Clark Corporation, Roswell, Georgia, USA) soaked in detergent solution and rinsed with 18 MΩ cm water. Tape is applied over one opening in the acrylic wall and 40 °C molten inclusion material is poured into the remaining opening filling the hole. Since the background is at room temperature, the inclusion material congeals within minutes.

After another 24 h to allow formaldehyde cross-linking of the inclusion material, a knife edge is used to cut the cylindrical inclusion flush with the sides of the phantom, and the phantom is removed from the acrylic-and-Saran-Wrap mould and submersed in safflower oil in a plastic container. The container is sealed with a cover. The cover is kept on except when elastograms are obtained to minimize long-term oxidation of the safflower oil.

3. Methods of measurement of material property values

At the time of manufacture of each component material in the phantoms, test samples were made for measurement of elastic, ultrasonic and NMR properties. For measurement of Young's moduli, 2.6 cm in diameter, 1.0-cm-thick sample discs were made. For ultrasonic measurements, 2.5-cm-thick, 7.6-cm-diameter samples are enclosed in a cylindrical container with 6-mm-thick acrylic walls and 25-μm-thick Saran Wrap® covering the parallel faces. For NMR relaxation time measurement, a 5-mm-diameter NMR tube is filled to within 5 mm of the top and is then sealed with petrolatum.

Young's moduli, ultrasonic parameters and NMR relaxation times were measured at 22 °C. The method for determining ultrasonic propagation speeds and attenuation coefficients is the commonly used through-transmission, water-substitution method described, e.g., in Madsen *et al* (1999).

For the 2.6-cm-diameter, 1.0-cm-thick samples of the TM materials, dynamic measurements of complex Young's moduli were made using an EnduraTEC 3200 ELF system (EnduraTEC Systems Corporation, Minnetonka, MN, USA) with a 250 g load cell. Test samples are kept immersed in safflower oil when measurements are not being made to prevent desiccation. To make a measurement, a sample disc is removed from the oil and placed between two horizontal parallel circular platens made of Teflon®. The platens are 3 cm in diameter. The lower platen has a circular lip around the edge assuring that the entire flat surfaces of the sample are in contact with the platens at all times. The inner diameter of the lip is 2.8 cm; thus, there is no constraint on the diameter of the sample. Residual safflower oil is left on the surfaces of the sample disc to assure that nearly frictionless slipping can occur at the interfaces between the platens and the sample disc.

The actual measurement procedure is programmed using the EnduraTEC WinTest:version 2.56® DMA (dynamic mechanical analysis) software (EnduraTEC Systems Corporation, Minnetonka, MN, USA). Initially, the upper platen is not in contact with the sample disc. It is lowered until contact is detected, and then the program completes the procedure as follows. After taring the load cell, the sample is compressed at 0.04 mm s^{-1} to a mean compression value M selected by the user and that compression is maintained for a user-selected time (typically 5 s) after which a 'precycle' compression variation is done ending at compression M. Then the sinusoidal oscillation in compression proceeds at a displacement amplitude chosen by the user. At least ten cycles are completed after which the Fourier analysis of both waveforms allows analysis at the peak frequency. Amplitudes of displacement and force are determined, as is the lag of the displacement relative to the force. These values, along with entered accurate values for the sample diameter and thickness, allow computation by the software of the real (storage) and imaginary (loss) parts of Young's modulus. At each frequency, the procedure is repeated once more and an averaging of the real and imaginary parts is taken. Then the compression is returned to the zero level of the chosen sinusoidal thickness variation. Frequencies employed were 0.1 and 1.0 Hz, the number of cycles being 10 and 100, respectively. Only 1 Hz values are reported in this paper; however, the difference between values at 0.1 Hz and 1.0 Hz is very small. Displacement and force are monitored simultaneously. With values of the diameter and thickness of the sample disc being introduced, the software then computes the real (storage) and imaginary (loss) parts of the complex Young's modulus.

At the time of production of each component material in a phantom, two disc samples were produced, called *production samples*. The Young's modulus for a component material is taken to be the mean Young's modulus for the pair. The standard error is taken to equal the sample standard deviation/$\sqrt{2}$ *unless* the resulting standard error is less than the estimated uncertainty for a single Young's modulus measurement (on a single sample), namely, 3% of the Young's modulus value, i.e., the minimum uncertainty for a mean Young's modulus value is 3% of that mean value. The 3% uncertainty for a single Young's modulus value corresponds to uncertainties of ± 0.2 mm in measurement of the height and diameter of the disc samples on which Young's modulus measurements are made.

The NMR relaxation times T_1 and T_2 were measured using the inversion-recovery pulse sequence for T_1 and the Carr–Purcell–Meiboom–Gill pulse sequence for T_2. The relaxometer employs a 60 MHz Bruker mq 60 minispec NMR analyser® (Bruker Optics, Inc., Minispec Division, The Woodlands, TX, USA) operating at a probe (sample) temperature of 22 °C. Monoexponential fitting sufficed for both T_1 and T_2.

4. Procedure for assessing long-term stability of the phantoms

The cylindrical inclusions have a different composition than their surroundings. Since inclusions and surroundings (background) are in direct contact, it is possible that significant changes in inclusion diameter and stiffness could occur over time because of osmotic effects.

4.1. Elastic contrast

Elastic contrast is defined as the ratio of the low frequency storage modulus (real part of the complex Young's modulus) of the inclusion to that of the background material. If a phantom is used in assessing strain imaging, it is important that the elastic contrast be known. If the phantom is to be used to test a system that aims to map the Young's modulus, then the complex Young's moduli for both materials composing the phantom must be known. The disc sample
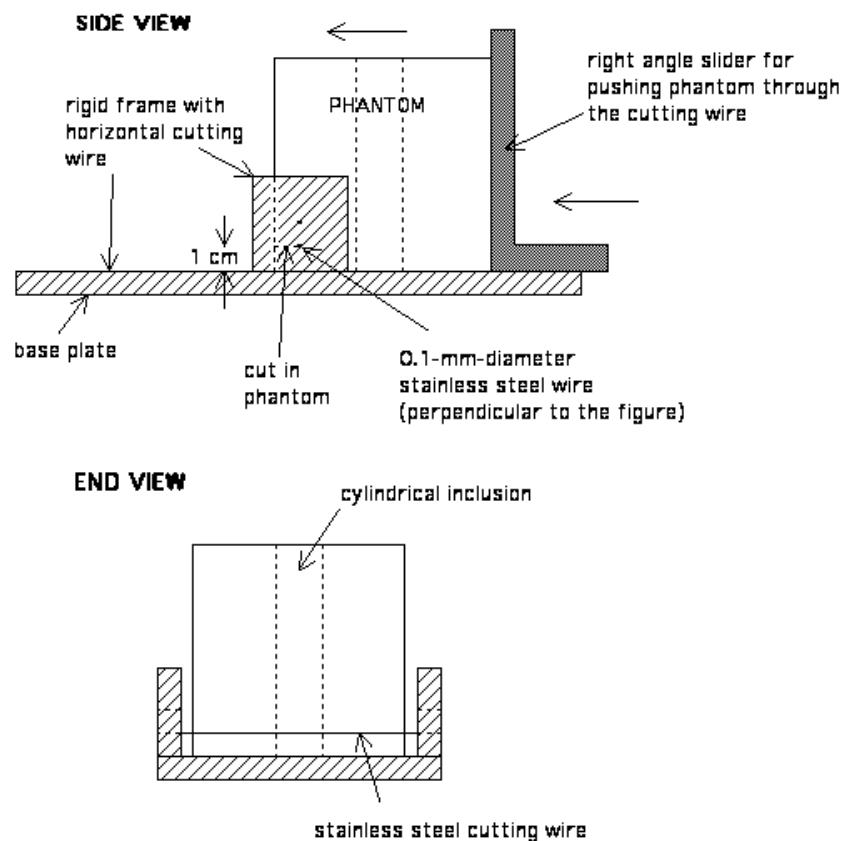
Figure 2. Diagrams of apparatus used to slice the phantoms to obtain samples for measurement of Young's modulus. The phantom is pushed through the cutting wire to obtain either 1-cm-thick or 2-cm-thick slices.

of a component material, made at the time each component of the phantom is made and referred to henceforth as a *production sample*, might be assumed to have the same complex Young's modulus as that in the phantom itself. However, because phantom components might change due to osmosis, it is necessary to test this assumption. This test was done by comparing storage moduli measured on the production samples with storage moduli of samples excised from the phantoms themselves (*excised samples*).

A version of 'cheese cutter' was used to excise samples from the heterogeneous phantoms for measurement of complex Young's moduli of the component materials (see figure 2). A rigid frame with a taut, horizontal 0.1-mm-diameter stainless steel wire positioned either 1 cm or 2 cm above a horizontal base plate constitutes the principal component of the apparatus. The phantom is placed on one side of the wire and a vertical slider surface is then used to push the phantom through the wire. The cylindrical inclusion of the phantom is oriented vertically so that the slice contains an inclusion disc in the centre. In figure 2 the wire is positioned to cut a 1-cm-thick slice.

After each slice was cut, the diameter of the inclusion disc was measured with a machinist's calipers; then 2 cm × 2 cm squares were cut from the background material of the slice and the 2-cm-diameter inclusion disc was excised with a razor blade. After each square or disc
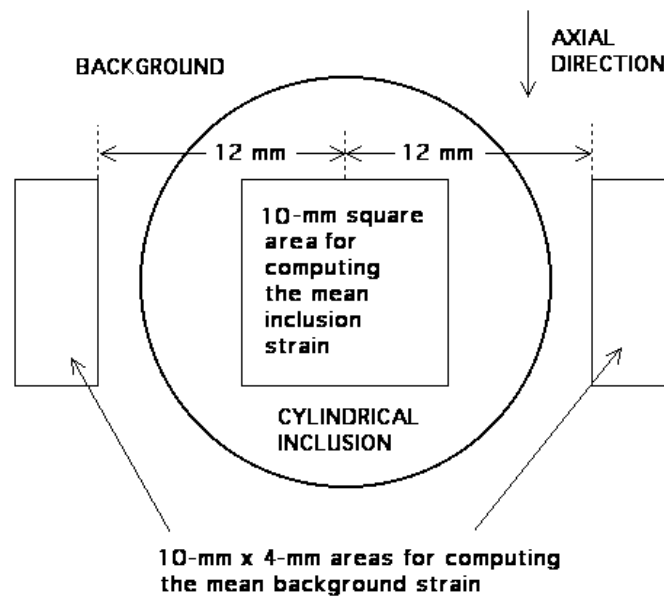
Figure 3. Diagram showing areas on elastograms for computation of strain ratios.

had been excised, it was immersed in safflower oil in a small labelled jar (with cap) until measurements were undertaken on the EnduraTEC 3200.

4.2. Strain ratios

The strain ratio is defined as the mean strain of the inclusion divided by the mean strain of the background. To assess the stability of the strain ratio, periodic determinations of strain ratios were made from elastograms of phantoms A-E obtained using an Aloka model SSD-2000 scanner with a 7.5 MHz linear array scan head. The focus was set at 5.5 cm for each determination.

The following method was followed for consistent selection of areas on the elastogram for determining mean strains (see figure 3). The centre of the inclusion is located on the elastogram and its pixel coordinates noted. Then the mean strain value and standard deviation are determined from all pixel values for pixels lying inside the 10 mm × 10 mm area. The standard error equals the standard deviation divided by the square root of the number of *independent* pixel values (strain values) (Bevington 1969). The number of strain values averaged is approximately $100 \, \text{mm}^2/[(4/22) \, \text{mm} \times (3/4) \, \text{mm}] \approx 733$ where (4/22) mm is the lateral pixel dimension and (3/4) mm is the axial pixel dimension. However, it is estimated that the number of *independent* pixels is 1/4 of 733 ≈ 180.

The mean strain value and standard deviation for the background are computed using the two 4 mm × 10 mm areas positioned relative to the 10 mm square area as shown in figure 3. Because the total area is 80% of that employed for the inclusion, the number of independent strain values is estimated to be 0.8 × 180 = 144.

Once the mean strain values and their standard errors for the inclusion and the background have been determined, the value of the strain ratio is computed. The error in its value is computed by straightforward propagation of errors using the computed standard errors for the inclusion mean strain and background mean strain.
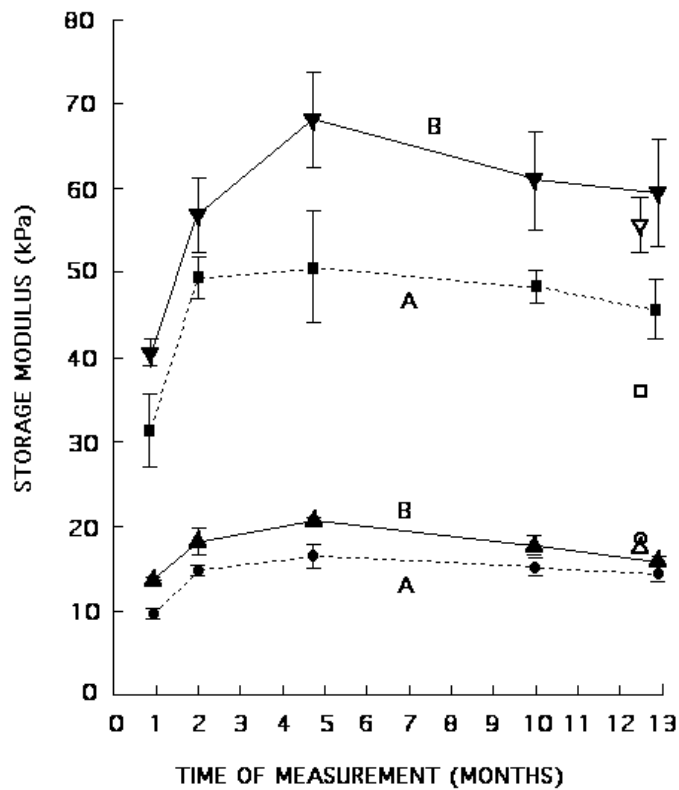
Figure 4. Mean storage moduli and standard errors for phantoms A and B. Production sample values are shown over a period of 1 year as filled triangles, circles or squares; inclusion values are shown as ■ for phantom A and ▼ for phantom B, and background values are shown as ● for phantom A and ▲ for phantom B. Mean storage moduli for inclusion samples cut from the phantoms are shown as □ for phantom A and ▽ for phantom B. Mean storage moduli for background samples cut from the phantoms are shown as ○ for phantom A and △ for phantom B.

4.3. Geometry

To test for size changes of inclusions due to osmosis, the cylinders were made (at the time of phantom production) with a diameter of 20.0 mm, and diameter measurements were made on slices cut from the phantoms many months after production as described in subsection 4.1. Typically, four independent inclusion diameter measurements were made with a machinist's calipers for each slice, and the uncertainty of the mean was taken to be the standard error. Diameter measurements were also made using ultrasound imaging prior to slicing up the phantoms.

5. Results

5.1. Mechanical properties

In figures 4–6, values for storage moduli are shown for the 2.6-cm-diameter, 1-cm-thick disc samples made at the time of production of each phantom component. Initial measurements were made within a few days of production of the corresponding phantom and continued for 9–12 months. The per cent compression was 2–6%.
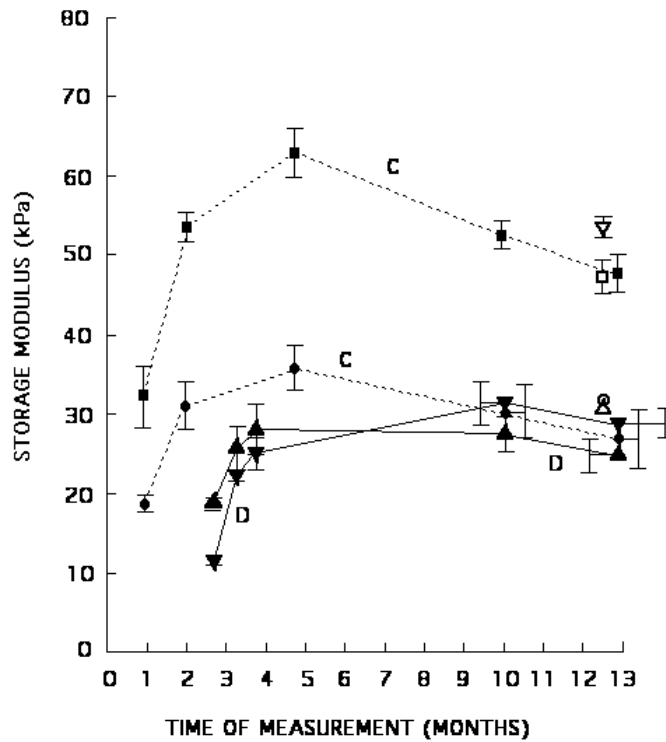
Figure 5. Mean storage moduli and standard errors for phantoms C and D. Production sample values are shown over a period of 12 months (phantom C) or 10 months (phantom D) as filled triangles, circles or squares; inclusion values are shown as ■ for phantom C and ▼ for phantom D, and background values are shown as ● for phantom C and ▲ for phantom D. Mean storage moduli for inclusion samples cut from the phantoms are shown as □ for phantom C and ▽ for phantom D. Mean storage moduli for background samples cut from the phantoms are shown as ○ for phantom C and △ for phantom D.

Also shown in figures 4–6 are the storage moduli for samples excised from each phantom 9–12 months after production of the phantom. The per cent compression was 2–4%.

For the production samples corresponding to each type of material, the value of tan $\delta \equiv$ (imaginary part of Young's modulus)/(real part of Young's modulus) = (loss modulus)/(storage modulus) does not demonstrate a time dependence when the material is at least 4 weeks old (see appendix A). Thus, it is considered sufficient to characterize the loss moduli of the production samples in terms of mean values and sample standard deviations over the time periods indicated in figures 4–6. Those values are given in table 2.

In table 3, means and standard errors of tan δ are shown for 1-cm-thick samples cut from the phantoms on one day followed by means and standard errors for 2-cm-thick samples cut the following day. The 2-cm-thick samples were produced to enhance accuracy of determination of complex Young's moduli.

Table 4 shows values of elastic contrasts determined in two ways. The first row of values corresponds to means of elastic contrast determined from the values of the storage moduli plotted in figures 4–6 over time. These values resulted from measurements made on the 2.6-cm-diameter, 1-cm-thick cylindrical production samples made at the time of production of each phantom component, i.e., these samples had never existed in one of the phantoms and, therefore, were never exposed to osmotic effects due to contact with materials of different
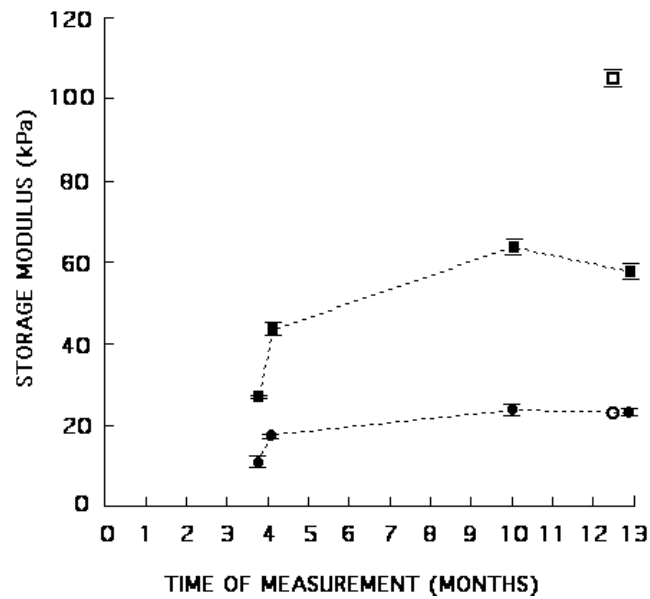
Figure 6. Mean storage moduli and standard errors for phantom E. Production sample values are shown over a period of nine months as filled circles or squares; inclusion values are shown as ■, and background values are shown as ●. The mean storage modulus for inclusion samples cut from the phantom is shown as □. The mean storage modulus for background samples cut from the phantom is shown as ○.

Table 2. The mean and standard errors of tan δ for the 1- cm-thick production samples over 6–12 months during which (complex) Young's moduli were measured. Initial tan δ values determined within 4 weeks of the phantom's production were excluded since they were 10–30% higher than the means for the remaining (later) tan δ values.

	Phantom A	Phantom B	Phantom C	Phantom D	Phantom E
Background	0.108 ± 0.023	0.097 ± 0.007	0.078 ± 0.004	0.070 ± 0.009	0.079 ± 0.007
Inclusion	0.121 ± 0.011	0.117 ± 0.010	0.096 ± 0.007	0.110 ± 0.013	0.122 ± 0.005

Table 3. Means and standard errors for tan δ corresponding to 1-cm-thick and 2-cm-thick samples cut from the phantoms. Note that the values for the 1-cm-thick samples are generally considerably greater than those for the 2-cm-thick samples.

	Phantom A	Phantom B	Phantom C	Phantom D	Phantom E
Background (1-cm cuts)	0.098 ± 0.010	0.126 ± 0.010	0.105 ± 0.005	0.121 ± 0.008	0.121 ± 0.008
Inclusion (1-cm cuts)	0.157 ± 0.008	0.152 ± 0.006	0.154 ± 0.021	0.154 ± 0.011	0.164 ± 0.009
Background (2-cm cuts)	0.095 ± 0.004	0.096 ± 0.004	0.075 ± 0.006	0.078 ± 0.003	0.078 ± 0.005
Inclusion (2-cm cuts)	0.119 ± 0.005	0.106 ± 0.017	0.096 ± 0.004	0.108 ± 0.005	0.120 ± 0.005

compositions. The second row of values consists of means of elastic contrast values determined from storage modulus values for the samples cut from slabs of the phantoms. The second row of values must be the correct values for the phantoms, of course.

There was a small nonlinearity in storage moduli observed. This was quantified by comparing measurements at 2–4% and 2–6% compressions on the same samples on the same day (the last day in figures 4–6). The results are shown in table 5.

Table 4. Elastic contrasts determined in two different ways. The means from samples excised from the heterogeneous phantoms must be correct.

Method of computing elastic contrast	Phantom identification				
	A	B	C	D	E
Mean from production samples ± stand error	3.17 ± 0.07	3.39 ± 0.10	1.75 ± 0.01	1.01 ± 0.07	2.55 ± 0.05
Mean from excised samples ± stand error	1.95 ± 0.05	3.18 ± 0.19	1.48 ± 0.08	1.74 ± 0.04	4.60 ± 0.10

Table 5. Assessment of storage modulus nonlinearity. Values of storage moduli for all ten production samples were determined on the last day shown in figures 4–6 at 2–4% and 2–6% compressions.

	Phantom A	Phantom B	Phantom C	Phantom D	Phantom E
Background (2–4%)	14.2 ± 1.0	16.0 ± 0.7	27.1 ± 3.1	25.1 ± 1.9	22.6 ± 1.2
Background (2–6%)	14.0 ± 0.9	15.8 ± 0.7	26.7 ± 3.3	24.9 ± 1.8	22.5 ± 1.2
Background per cent change	−1.4%	−1.3%	−1.5%	−0.8%	−0.4%
Inclusion (2–4%)	43.3 ± 3.3	57.7 ± 6.4	47.0 ± 2.5	27.8 ± 1.6	56.2 ± 1.7
Inclusion (2–6%)	45.5 ± 3.4	59.2 ± 6.3	47.8 ± 2.5	28.6 ± 1.6	57.6 ± 1.8
Inclusion per cent change	+4.9%	+2.6%	+1.7%	+2.1%	+2.5%

Table 6. Inclusion diameters measured near the mid-plane of the phantoms using ultrasound imaging and directly on slices cut from the heterogeneous phantoms. Also shown is the estimated increase in volume relative to the initial 20.0-mm-diameter cylinder.

Phantom identification	Axial diameter using ultrasound (mm)	Mean diameter of cut specimen (mm)	Estimated per cent increase in cylinder volume using cut specimen diameter
A	21.4	21.9 ± 0.1	20 ± 1
B	20.6	21.0 ± 0.2	10 ± 2
C	21.1	21.3 ± 0.1	13 ± 1
D	21.0	21.1 ± 0.2	11 ± 2
E	20.4	20.5 ± 0.1	5 ± 1

In figures 7 and 8, values of the strain ratio for all five phantoms obtained over a period of many months are shown. The initial strain ratio for each phantom was obtained 3–6 weeks after production of the phantom. The horizontal dashed lines correspond to the mean values of the plotted strain ratio values for each phantom. The location of the letter P on each dashed line indicates the time of production of that phantom.

5.2. Geometry

Table 6 shows values for the diameters of the inclusions measured directly with a machinist's calipers and with ultrasound imaging using electronic calipers along the axial direction. Ultrasonic and direct measurements were made in the same 5-day period.

5.3. Ultrasound and NMR properties

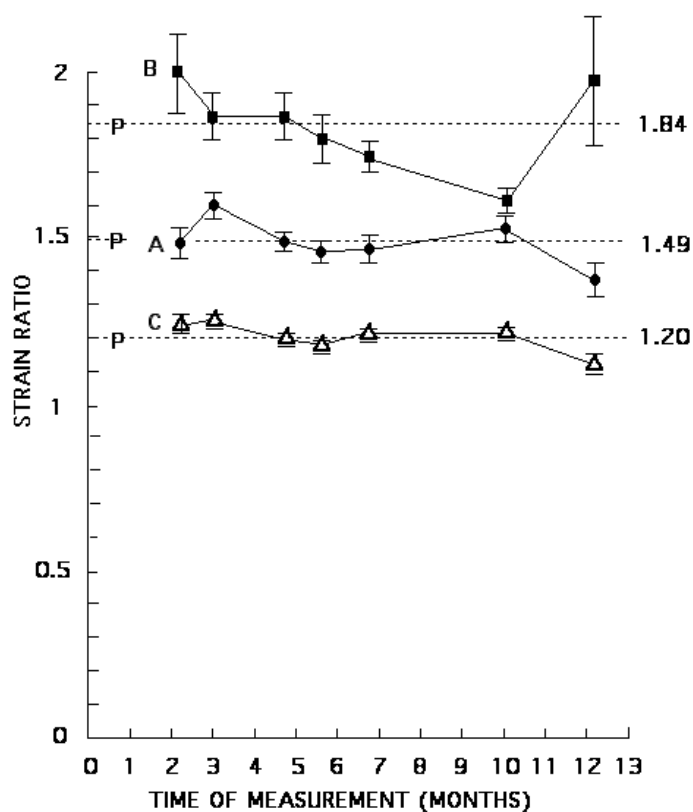In table 7, values for ultrasound and NMR properties are shown.

Figure 7. Strain ratios obtained from elastograms over a 10 month period for phantom A (●), phantom B (■) and phantom C (△). The dashed horizontal lines correspond to the mean of all strain ratios for each phantom, the numerical value appearing on the right side. The position of the letter P on each dashed line indicates the time of production of the phantom.

Table 7. Ultrasound and NMR properties measured at 22 °C on samples of each of the ten different materials formed at the time of production of each material. Density values were computed based on knowledge of densities of component materials.

|	Ultrasound properties			NMR relaxation times	
TM material version	Propagation speed (m s^{-1})	Atten. coeff. ÷ frequency (dB cm^{-1} MHz^{-1})	Density (g ml^{-1})	T_1 (ms)	T_2 (ms)
Phantom A BKGD	1518 ± 1	0.35 ± 0.02	1.04	498.2 ± 0.2	63 ± 2
Phantom A INCL	1527 ± 1	0.45 ± 0.02	1.05	431 ± 5	28.4 ± 0.2
Phantom B BKGD	1526 ± 1	0.35 ± 0.02	1.04	456.6 ± 0.5	60 ± 2
Phantom B INCL	1533 ± 1	0.47 ± 0.02	1.05	402.3 ± 0.4	28.8 ± 0.3
Phantom C BKGD	1532 ± 1	0.36 ± 0.02	1.04	419 ± 1	59 ± 1
Phantom C INCL	1542 ± 1	0.50 ± 0.02	1.05	369 ± 1	32.7 ± 0.5
Phantom D BKGD	1532 ± 1	0.38 ± 0.02	1.04	423.0 ± 0.8	57 ± 1
Phantom D INCL	1535 ± 1	0.14 ± 0.02	1.00	494 ± 2	59 ± 1
Phantom E BKGD	1518 ± 1	0.46 ± 0.02	1.04	396 ± 1	59 ± 1
Phantom E INCL	1518 ± 1	0.18 ± 0.02	1.00	488 ± 1	53 ± 1
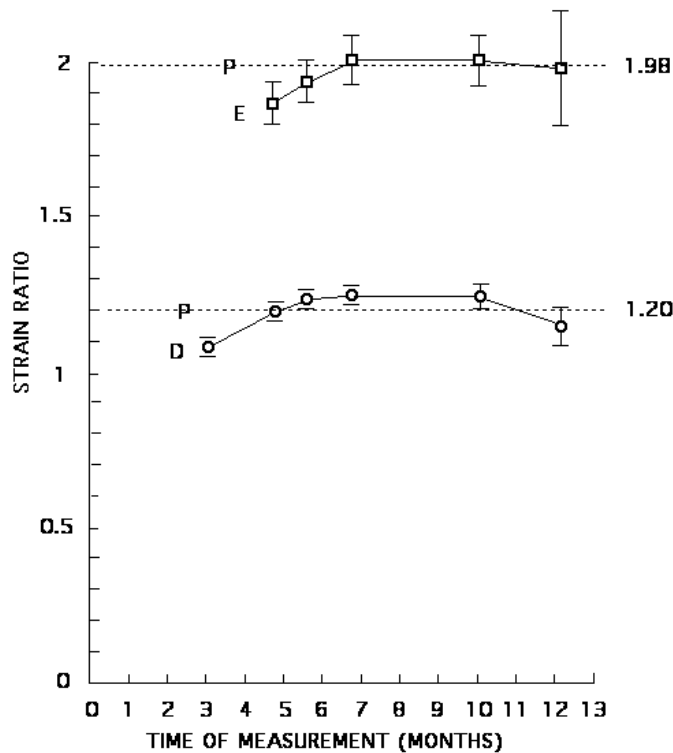
Figure 8. Strain ratios obtained from elastograms over a 9 month period for phantom D (○) and a 7 month period for phantom E (□). The dashed horizontal lines correspond to the mean of all strain ratios for each phantom, excluding the initial values in each case. The numerical mean value corresponding to the dashed line appears at the right end of the line. The position of the letter P on each dashed line indicates the time of production of the phantom.

6. Discussion

6.1. Storage moduli

The storage moduli of the production samples (produced at the time of production of each phantom component) are shown over a 9 to 12 month period in figures 4–6 (closed circles, triangles and squares). The storage moduli rise considerably during the first few months and then gradually decrease.

The storage moduli for the samples cut from the phantoms are also shown in figures 4–6 (open circles, triangles and squares). Those storage moduli of samples cut from the backgrounds agree rather well with those of the background production samples measured at the same time. However, for storage moduli of the inclusions that level of agreement exists only for phantoms B and C. Assuming that the (mean) storage modulus for the inclusion samples cut from the phantom is the correct value, the production sample values for phantoms A, D and E are, respectively, high by 27%, low by 47% and low by 45%. Thus, values of storage moduli for the inclusion production samples should not be assumed to correspond to the storage moduli of the inclusion material in the actual phantom.

In figure 5, the values of storage moduli measured over time for the inclusion production samples for phantom D are confusing. Based on compositions, the inclusion storage moduli

might be expected to be nearly the same as those for phantom C. As seen in table 1, the major difference in composition between phantoms C and D is that there are no beads in the inclusion material of phantom D, while there are beads in the inclusion material of phantom C. The inclusion storage moduli for phantom D (figure 5) are far below those for phantom C. In fact, earlier inclusion storage moduli for phantom D are lower than the corresponding background values and end up only slightly higher. On the other hand, the mean storage moduli for inclusion samples cut from phantom D agree with both cut and production samples for phantom C, as would be expected. One possible explanation for the unexpected storage modulus values for the inclusion production samples of phantom D is that there was a mix up of samples in the laboratory, i.e., the production samples measured did not actually correspond to the inclusion material in phantom D. Another possible explanation is that the two production samples corresponding to the inclusion material of phantom D were accidentally placed close to a laboratory heating source and their temperature became elevated enough to cause chemical change with no visual evidence that heating had occurred.

A small nonlinearity was observed for the storage moduli when results for a compression range of 2–4% were compared with results for a range of 2–6% (table 5). An average decrease of about 1% for the five background samples occurred with higher compression range while an increase of about 2.8% occurred for the five inclusion samples. (However, excluding phantom A from the average, the average increase for the inclusion samples was 2.2%.) The higher dry-weight concentration of agar in the inclusions may account for the increase for the inclusion samples, agar *per se* being nonlinear (Hall *et al* 1997).

The lack of validity of inclusion storage moduli of the production samples is reflected in the computed elastic contrast values shown in table 4. The elastic contrasts computed from the storage moduli of the samples cut from the samples should be the correct values for the phantoms.

6.2. Loss moduli and tan δ values

Referring to table 3, where tan δ values are shown for 1-cm-thick and 2-cm-thick samples cut from the phantoms, tan δ values for the 1-cm-thick samples are generally considerably greater than those for the 2-cm-thick samples, even though the storage moduli for the 1-cm and 2-cm samples agree very well for each of the ten different materials. Thus, there is a significant partial loss due to slipping friction at the platens, and that part of the loss should not be counted in the loss moduli or tan δ values.

The correct values of the loss modulus—or equivalently tan δ—can be computed from the values in table 3 using the following facts: (1) The ratio of the amplitude of the sinusoidal oscillation to the sample thickness was kept the same, namely, 0.01. (2) The parallel flat areas contacting the platens were all the same. (3) The Young's modulus is an intrinsic material property. The applicable relations are

$$E'' = 2E''_{2\text{-cm}} - E''_{1\text{-cm}} \qquad \text{and} \qquad \tan \delta = 2 \tan \delta_{2\text{-cm}} - \tan \delta_{1\text{-cm}} \qquad (1)$$

where E'' and $\tan \delta$ are the computed best estimates for the loss modulus and tan δ, $E''_{1\text{-cm}}$ is the loss modulus determined experimentally using the 1-cm-thick cut sample, etc (see appendix B for a derivation of equations (1)). With propagation of errors, the corrected (computed) mean values and standard errors of tan δ are given in table 8.

The derived (corrected) values of tan δ for phantom A are a little larger than for the other four phantoms. Recall that all phantoms except phantom A were preserved with Germall-plus®, phantom A being preserved with thimerosal.

Note that the measured tan δ values for the production samples shown in table 2 are less than those for the equal thickness (1 cm) samples cut from the phantom (table 3). This likely

Table 8. Mean values and standard errors for tan δ of the ten materials in the five phantoms derived from table 3 to eliminate the loss due to slipping friction at the platens.

	Phantom A	Phantom B	Phantom C	Phantom D	Phantom E
Backgrounds	0.092 ± 0.013	0.066 ± 0.013	0.045 ± 0.013	0.035 ± 0.010	0.035 ± 0.013
Inclusions	0.081 ± 0.013	0.060 ± 0.013	0.038 ± 0.022	0.063 ± 0.015	0.076 ± 0.013

is because the wire-cut surfaces of the cut samples were rough in comparison to the moulded production sample surfaces.

6.3. Strain ratios

Strain ratios monitored periodically for seven to ten months are shown in figures 7 and 8. These results indicate that the strain ratios are temporally stable. Only one strain ratio value of the 32 values plotted might be of concern, namely, the tenth month value for phantom B (figure 7). That value is 87% of the mean of 1.84 for all seven values, and the error bars are small; we do not have an explanation for this lower value. Another value, the first obtained for phantom D, is 90% of the mean of all six values; however, that first value was obtained only two weeks after production of that phantom.

Each phantom was cut up for direct measurement of cylinder diameter and for determination of Young's moduli from the materials in the phantom (see section 6.4). Thus, how long these phantoms would be useful after completion of this study is not known. However, in the case of phantom E, a phantom containing arrays of small spherical simulated lesions (diameters 1.6, 2, 3 and 4 mm) was made at the same time using the same materials (Madsen *et al* 2005). At the time of writing, this phantom is 15 months old and is still in use for monitoring the performance of elastography systems, and results continue to be consistent with stability of elastic contrast and geometry.

6.4. Elastic contrast

Stability of strain ratios also implies that elastic contrasts possess long-term stability. Thus, it is reasonable to assume that the elastic contrast obtained by measuring the storage moduli of samples cut from a phantom 2–12 months after production is an accurate estimate of the elastic contrast for that phantom over the entire 10 month period.

The stability of elastic contrast and its determinability using samples cut from an agar/gelatin phantom in which the volume of the inclusion is much less than the volume of the background can be utilized to determine the true elastic contrast of any heterogeneous agar/gelatin phantom for which the total inclusion volume is much less than the background volume. For example, suppose a 'spherical lesion' phantom is made in which an array of small spheres have an agar concentration greater than that of the background. If a phantom with the geometry shown in figure 1 is made at the same time using the same materials that compose the spherical lesion phantom, then the elastic contrast determined from samples cut from the cylinder phantom should equal that for the spherical lesion phantom.

6.5. Specification of storage moduli

Some researchers will want to know the actual storage modulus values for background and inclusions so that the phantom is useful regarding derivation of the storage moduli from

strain ratios. If production samples corresponding to the background material are made and it is accepted that the elastic contrast is invariant, then determination of the elastic contrast using samples cut from a cylinder phantom plus the value of the storage modulus of the background at the time of concern allow computation of the storage modulus of the inclusion(s).

6.6. Geometry

Referring to table 6, all cylindrical inclusions increased in diameter from an initial value of 20.0 mm at the time of production. The greatest diameter increase occurred for phantom A. Phantom A is not very important, however, because the preservative used was thimerosal, a mercury-containing compound used in past phantoms. The more environmentally acceptable Germall-plus has been shown to be an excellent alternative to thimerosal; therefore, future phantoms will be preserved with Germall-plus instead of thimerosal. The mean diameter increase for phantoms B–D was 1 mm, about 5%, and the mean volume increase was 10%. These are small increases. Thus, if a spherical lesion phantom were produced with 3.0-mm-diameter spherical inclusions, then a sphere volume increase of 10% corresponds to a diameter increase from 3.0 to 3.1 mm, a tolerable difference.

The fact that no perceptible changes in size of inclusions were observed for low MR contrast phantoms (Madsen *et al* 1991) described in section 1 may be related to two factors: first, the MR phantoms were low contrast so that the dry-weight agar concentrations in the inclusions were closer to that in the surroundings than in the present study; second, the uncertainties in the MR determinations of sizes were greater than in the case of modern ultrasound or direct measurement with machinist's calipers done in the current study.

6.7. Ultrasound properties

Since the values for these properties were measured on 'production' samples made at the time of production of the respective phantom components, only values for the background materials can be assumed accurate. However, since the increases in volume of inclusions in the phantoms are only about 10%, it is reasonable that ultrasound properties determined for the inclusion materials are not greatly in error. If more accurate values of ultrasound attenuation coefficients and propagation speed for the inclusion material are considered essential for some use of the phantom, then samples cut from the cylinder phantom for determination of Young's moduli could also be used to measure those ultrasound properties.

Note that the slopes of the ultrasound attenuation coefficient versus frequency for the background materials of all five phantoms lie in the range 0.35–0.46 dB cm^{-1} MHz^{-1} at 22 °C, a good approximation for the attenuation of many soft tissues.

The ultrasound propagation speeds in the background materials range from 1518 through 1532 m s^{-1} at 22 °C. If values closer to 1540 m s^{-1} are desired, an appropriate concentration of glycerol can be included in both background and inclusions during manufacture of the phantom.

We have used small concentrations of glycerol to raise propagation speeds in ultrasound phantom materials. The rate of increase is about 4.4 m s^{-1} per weight per cent glycerol. For weight per cent concentrations of up to 10%, the increase in attenuation coefficient slope is less than 0.02 dB cm^{-1} MHz^{-1}. To adjust a speed from 1518 m s^{-1} to 1540 m s^{-1} would require a 5% glycerol concentration. Thus, ultrasound attenuation should not be affected. It seems likely that mechanical properties would not be significantly affected at this low concentration either.

6.8. NMR properties

In the case of phantoms A, B and C, both T_1 and T_2 are lower for the inclusion material than for the background material. This is expected because of the higher concentration of agar in the inclusion material. However, this expected distinction between inclusion and background materials is not demonstrated for phantoms D and E. For these phantoms, T_1 actually is higher in the inclusions than in the background and T_2 is about the same.

A major difference between the phantoms is that in phantoms A–C the inclusions have a rather high concentration of glass beads (about 5.5% by weight), while there are no beads in the inclusion of phantom D and a relatively small concentration in the inclusion of phantom E (see table 1). All five phantoms have a bead concentration of 3.4–4.6% by weight in the backgrounds. Probably the glass beads contribute to lowering T_1 and T_2. If the magnetic susceptibility of the glass beads is sufficiently different from that of the surrounding gel, then the T_2 value measured is actually T_2^*, which depends on settings of the pulse spacing of the CPMG pulse sequence. Thus, T_2^* is not an acceptable specification of the T_2 intrinsic to materials.

An experiment was carried out on a sample with a higher concentration of glass beads (inclusion material for phantom B) to see if the measured T_2 value depended on the CPMG pulse separation. Using the usual pulse separation of 2.5 ms, the T_2 value was 27.4 ms. With pulse separations of 1 ms, 0.2 ms and 0.1 ms, the T_2 values determined were 31.3 ms, 39 ms and 41 ms, respectively, indicating that the beads were lowering measured T_2 values due to diffusion effects and non-tissue-like local variations in magnetic permeability. Thus, if phantoms are to be considered tissue-mimicking for use in MR elastography, there should be no glass beads present.

7. Summary and conclusions

Five phantoms with a variety of compositions were made using a base material of agar, gelatin, water, formaldehyde, Cu^{2+}, EDTA, NaCl, microscopic glass beads and a preservative. Cylindrical inclusions existed in each phantom with higher dry-weight agar concentrations than in the background material. The dry-weight gelatin concentration was constant throughout each phantom. The volume fraction corresponding to the cylindrical inclusions was small— about 4%. The phantoms are tissue-mimicking with respect to mechanical and ultrasound properties, but adequate mimicking of NMR relaxation times is compromised by the presence of microscopic glass beds used to increase ultrasound attenuation. Agar/gelatin phantoms for use in MR elastography should be made without glass beads.

Changes in the inclusions for about 1 month following production were probably caused by osmotic effects. These changes included an approximately 10% increase in cylinder volume and a significant change in Young's modulus compared to the value for samples of inclusion material not subject to osmotic effects (never in contact with background material). Thus, the true Young's modulus of the cylindrical inclusion must be determined using a sample cut from the phantom.

Note that tan δ for the materials in these phantom materials is small—about 0.05.

Monitoring of the strain ratio for the five phantoms over 7–10 months indicated long-term stability of that parameter. Stability of strain ratio implies stability of elastic contrast also. Thus, elastic contrast for a phantom can be determined by measuring the storage modulus of inclusion and background materials excised from the phantom, allowing 1 or 2 months after production of the phantom for chemical stability to be established.

7.1. Characterization of phantoms with inclusions of any size and number but a small total volume fraction

Phantoms for testing the performance of elastography systems are not restricted to ones with cylindrical inclusions. For example, one type of phantom (Madsen *et al* 2004) has arrays of small spherical inclusions in a background material, the total volume fraction of inclusions being much less than 4%. It is not practical to try to measure the inclusion storage modulus using samples cut from the small spheres since the spheres are 5 mm or less in diameter. However, if a phantom of the geometry in figure 1 is made at the same time as the spherical lesion phantom with the background and 2-cm inclusion diameter cylindrical inclusion composed of the same materials as in the spherical lesion phantom, then samples can be cut from the cylinder phantom after 2 months to determine the storage modulus of background and inclusion and, therefore, the elastic contrast for both the cylinder and spherical lesion phantom.

　　Some researchers in elastography are interested in deriving the storage modulus distribution using the strain ratio elastogram. Following is a method for determining the storage moduli for background and inclusions in these phantoms at any time following production of the phantom. Although the elastic contrast in the phantoms is stable, the actual values of the storage moduli for the background material rise and then fall over at least a year. (See background storage moduli in figures 4–6.) If samples of background material for measurement of the storage modulus are produced at the time of production of a phantom, a measurement of the storage modulus of these background samples at any time, plus knowledge of the elastic contrast, allows computation of the storage modulus of the inclusion material at that time.

7.2. Method of preservation

There appears to be no advantage to the use of thimerosal as a preservative while there is a considerable disadvantage since thimerosal is a mercury-containing compound. Thus, preservation with Germall-Plus® is recommended.

Acknowledgments

Appendix A

Values of tan δ versus time after production are given in table A1 for the phantom C production samples. These demonstrate the lack of time dependence of tan δ when the samples are at least 4 weeks old. Note that the largest values for both background and inclusion occur at 1 week after production.

Appendix B

There is an error in the measured loss modulus, E'', and therefore also in tan δ due to slipping friction at the interface between the platens and sample. Following is a way to compute corrected values of E'' and tan δ when measurements of Young's moduli of samples differing only in thickness are available. Samples with the same area and thicknesses of 1 cm and 2 cm

Table A1. Values of tan δ versus time lapse since production for the production samples corresponding to phantom C.

Material	Number of weeks after production of the phantom and production samples				
	1	6	14	41	52
Background	0.087	0.073	0.078	0.083	0.077
Inclusion	0.121	0.103	0.094	0.087	0.098

cut from the phantoms were available. The per cent compression range used for both was the same, namely, 2–4%. The (complex) Young's modulus E is defined by

$$\Delta F/A = E\,\Delta z/z \tag{B.1}$$

where ΔF is the sinusoidally varying force, A is the mean sample area, Δz is the sinusoidally varying displacement and z is the sample thickness. For notational brevity, define $\Delta P \equiv \Delta F/A$ and $\Delta C \equiv \Delta z/z$. Then equation (B.1) becomes

$$\Delta P = E\,\Delta C. \tag{B.2}$$

We have $\Delta P = (\Delta P)_\text{o}\,\mathrm{e}^{\mathrm{i}\omega t}$ and $\Delta C = (\Delta C)_\text{o}\,\mathrm{e}^{\mathrm{i}(\omega t - \delta)}$, $\delta \geqslant 0$, where δ is the phase lag of displacement due to energy loss in the material. Then

$$E = \Delta P/\Delta C = (\Delta P)_\text{o}/(\Delta C)_\text{o}\,\mathrm{e}^{\mathrm{i}\delta} = E' + \mathrm{i}E'' \tag{B.3}$$

where $(\Delta P)_\text{o}$ and $(\Delta C)_\text{o}$ correspond to real-valued amplitudes, E' is the (real) storage modulus, E'' is the (real) loss modulus and $i \equiv \sqrt{-1}$. Also, $\tan\delta = E''/E'$.

The energy loss per cycle for a disc of mean area A and mean thickness z, *not counting slipping frictional loss at the platens*, can be computed as a function of E'' and $(\Delta C)_\text{o}$. Consider the real force applied by the platen at the one moving surface $\Delta F_\text{R} = (\Delta P)_\text{o} A \cos\omega t$ (The other surface is assumed to be stationary) and the real displacement at that surface $\Delta z_\text{R} = (\Delta C)_\text{o} z \cos(\omega t - \delta)$. Thus the energy loss per cycle, ignoring frictional loss at the platens, is

$$\begin{aligned}
L &= \int_{\text{one cycle}} \Delta F_\text{R}\,d(\Delta z_\text{R}) \\
&= -(\Delta P)_\text{o} A(\Delta C)_\text{o} z\omega \int_0^{2\pi/\omega} \cos(\omega t)\sin(\omega t - \delta)\,\mathrm{d}t \\
&= (\Delta P)_\text{o} A(\Delta C)_\text{o} z\pi \sin\delta,
\end{aligned} \tag{B.4}$$

and the loss per cycle per unit volume, ignoring friction at the platens, is

$$L/(Az) = (\Delta P)_\text{o}(\Delta C)_\text{o}\pi \sin\delta = \pi E''(\Delta C)_\text{o}^2 \tag{B.5}$$

where $E'' = (\Delta P)_\text{o}/(\Delta C)_\text{o} \sin\delta$ has been imported from equation (B.3).

Since the values of A and $(\Delta C)_\text{o}$ are assumed to have been made the same experimentally for samples of different thicknesses, the energy loss per cycle due to slipping friction at the platens, L_F, must be the same for both thicknesses. Let the thickness of one sample, z_2, be twice the thickness of the other sample, z_1; then $z_2 = 2z_1$. Thus, the actual energy loss per cycle, *including slipping frictional loss at the platens*, is $L_2 = (\Delta P)_\text{o} A(\Delta C)_\text{o} z_2\pi \sin\delta + L_\text{F}$ for the sample of thickness z_2 and $L_1 = (\Delta P)_\text{o} A(\Delta C)_\text{o} z_1\pi \sin\delta + L_\text{F}$ for the sample of thickness z_1.

The *measured* loss moduli are

$$E_1'' = \left[\pi(\Delta C)_o^2\right]^{-1}[(L_1 + L_F)/(Az_1)] = E'' + L_F\left[\pi(\Delta C)_o^2 Az_1\right]^{-1} \qquad \text{(B.6)}$$

and

$$E_2'' = \left[\pi(\Delta C)_o^2\right]^{-1}[(L_2 + L_F)/(Az_1)] = E'' + L_F\left[\pi(\Delta C)_o^2 Az_2\right]^{-1} \qquad \text{(B.7)}$$

for sample thicknesses z_1 and z_2, respectively, where E'' is the correct loss modulus.

Introducing the assumption that $z_2 = 2z_1$, equations (B.6) and (B.7) can be solved for the correct loss modulus, E'' in terms of E''_1 and E''_2, namely,

$$E'' = 2E_2'' - E_1''. \qquad \text{(B.8)}$$

If the storage moduli determined for the two thicknesses are the same (They were for the 1-cm and 2-cm-thick cut samples.) and are assumed to be correct, then

$$E''/E' = 2E_2''/E' - E_1''/E' \qquad \text{or} \qquad \tan\delta = 2\tan\delta_2 - \tan\delta_1 \qquad \text{(B.9)}$$

where $\tan\delta_1$ corresponds to the measured value for the sample of thickness z_1 and $\tan\delta_2$ corresponds to the measured value for the sample of thickness z_2.

References

Bevington P R 1969 *Data Reduction and Error Analysis for the Physical Sciences* (New York: McGraw-Hill)

de Korte C L, Cespedes E L, van der Steen A F W, Norder B and te Nijenhuis K 1997 Elastic and acoustic properties of vessel mimicking material for elasticity imaging *Ultrason. Imaging* **19** 112–26

Gao L, Parker K J and Alam S K 1995 Sonoelasticity imaging: theory and experimental verification *J. Acoust. Soc. Am.* **97** 3875–86

Hall T J, Bilgen M, Insana M F and Krouskop T A 1997 Phantom materials for elastography *IEEE Trans. Ultrason. Ferroelectr. Freq. Control* **44** 1355–65

Kallel F, Prihoda C D and Ophir J 2001 Contrast-transfer efficiency for continuously varying tissue moduli: simulation and phantom validation *Ultrasound Med. Biol.* **27** 1115–25

Madsen E L, Blechinger J C and Frank G R 1991 Low-contrast focal lesion detectability phantoms for ^{1}H MR imaging *Med. Phys.* **18** 549–54

Madsen E L *et al* 1999 Interlaboratory comparison of ultrasonic backscatter, attenuation and speed *J. Ultrasound Med.* **18** 615–31

Madsen E L *et al* 2004 Tissue-mimicking spherical lesion phantoms for elastography with and without ultrasound refraction effects *Proc. Third Int. Conf. on the Ultrasonic Measurement and Imaging of Tissue Elasticity (Lake Windermere, Cumbria 17–20 Oct 2004)* p 102

Madsen E L, Frank G R, Hobson M A, Shi H, Jiang J, Varghese T and Hall T J 2005 Spherical lesion phantoms for testing the performance of elastography systems *Phys. Med. Biol.* submitted

Madsen E L, Frank G R, Krouskop T A, Varghese T, Kallel F and Ophir J 2003 Tissue-mimicking oil-in-gelatin dispersions for use in heterogeneous phantoms *Ultrason. Imaging* **25** 17–38

Plewes D B, Bishop J, Samani A and Sciarretta J 2000 Visualization and quantification of breast cancer bio-mechanical properties with magnetic resonance elastography *Phys. Med. Biol.* **45** 1591–610

Rice J R, Milbrandt R H, Madsen E L, Frank G R and Boote E J 1998 Anthropomorphic ^{1}H MRS head phantom *Med. Phys.* **25** 1145–56